Journal of Alloys and Compounds 509 (2011) 3880–3885

Contents lists available at ScienceDirect

Journal of Alloys and Compounds

journal homepage: www.elsevier.com/locate/jallcom

Spherical granular structures of Ag/Co nanoparticles: Synthesis, characterization and magnetic properties

P. Saravanan [a,*], K. Srinivasa Rao [b], M. Premkumar [a], A.K. Singh [a]

[a] Defence Metallurgical Research Laboratory, Hyderabad 500058, India
[b] Centre for Materials for Electronics Technology, Hyderabad 500051, India

ARTICLE INFO

Article history:
Received 7 July 2010
Received in revised form 9 December 2010
Accepted 10 December 2010
Available online 28 December 2010

Keywords:
Colloidal nanoparticles
Bimetallic
Ag/Co
Granular alloys
Spherical aggregates
Polyol process

ABSTRACT

Ag/Co bimetallic nanoparticles in the form of hierarchical spherical structures were prepared by the polyol process using oleic acid and oleylamine as surfactants. The Ag/Co nanoparticles so obtained were characterized by X-ray diffraction (XRD), field-emission scanning electron microscope (FESEM), transmission electron microscope (TEM), UV–vis spectroscopy (UV–Vis), small angle X-ray scattering (SAXS), vibrating sample magnetometer (VSM) and super-conducting quantum interference device (SQUID). The XRD results in complement with the UV–vis studies indicated the absence of Ag–Co alloy formation during the synthesis. The FESEM observations depicted dense and uniform spherical granular structures for the Ag/Co nanoparticles; while the TEM studies apparently revealed a bimodal distribution of nanoparticles exist in the Ag/Co samples. The SAXS analysis on the Ag/Co colloids further validated the TEM results. The VSM studies showed typical ferromagnetic characteristics for the Ag/Co nanoparticles at room temperature; whereas the SQUID measurements demonstrated superparamagnetic nature for these nanoclusters with a blocking temperature close to 250 K. The synthetic route presented in this work represents a simple means of producing bimetallic composite superstructures of Ag/Co nanoparticles in the form of spherical granules on a large scale. These spherical aggregates have the potential to be important building blocks for more complex nanostructures and would be interesting for magnetic studies and catalytic applications.

1. Introduction

Much attention has been paid on the nanocrystalline alloys of noble-ferromagnetic immiscible metal systems such as Ag–Co, Ag–Fe and Ag–Ni, owing to their interesting physical properties and applications in magnetic recording, optical devices and sensors [1–4]. The formation of nanocrystalline alloys of immiscible metals can be achieved through non-conventional techniques such as sputtering, thermal evaporation, ion-beam mixing, laser ionization and electrodeposition [5–8]. These nontraditional methods facilitate the synthesis of particles in the nanometer size range and allow the fabrication of alloys from the immiscible metals. Nevertheless, the particle size of the nanosized or the granular alloys prepared by these techniques is rather large and may not be suitable for realizing sizable giant magneto-resistance (GMR). Both particle size and their separation are the key parameters, which affect the GMR characteristics and of course, these parameters must be smaller than the spin-dependent electron mean free path [9].

Of relevant interest when using the nanosized alloys, is how to decrease the particle size of the material. Generally, particle size of the nanosized alloys prepared by the vapor or the sputter deposition and the melt quenching is rather large [10]. In this context, a great deal of attention has been focused on the granular alloys, employing numerous chemical methods including sol–gel, metal salt reduction and thermal decomposition. For instance, it is known that Ag and Co are immiscible in all proportions due to the difference in surface free energy and large atomic size differences. The segregation between Co and Ag occurs because of the surface free energy of Co (2.71 J/m^3) is more than twice as that of Ag (1.30 J/m^3) causing the Co to cluster [11]. There is a very poor lattice match since FCC-Ag has lattice parameter that is 15% larger than that of FCC-Co. The heat of formation between Co and Ag is positive (+26 kJ/g atom) so that there is no tendency for the formation of the compound Ag–Co or for alloying [12]. Nevertheless, with the aid of chemical methods, the formation of Ag–Co granular alloys can have three possibilities [13]: (i) core–shell type particles, Ag-core with Co-shell or vice versa [14]; (ii) phase-separated composites, which are made of partly Ag and partly of Co; and (iii) physical mixture of mono-metal particles [15]. A series of nanocrystalline Co_xAg_{100-x} solid solutions with average particle size of ~20 nm have been prepared by $NaBH_4$ reduction of their corresponding metal salts at room temperature

* Corresponding author at: Defence Metallurgical Research Laboratory, Hyderabad 500058, A.P., India. Tel.: +91 40 24586820; fax: +91 40 24340884.
E-mail addresses: psdrdo@gmail.com, ps@dmrl.drdo.in (P. Saravanan).

0925-8388/$ – see front matter © 2010 Elsevier B.V. All rights reserved.
doi:10.1016/j.jallcom.2010.12.141

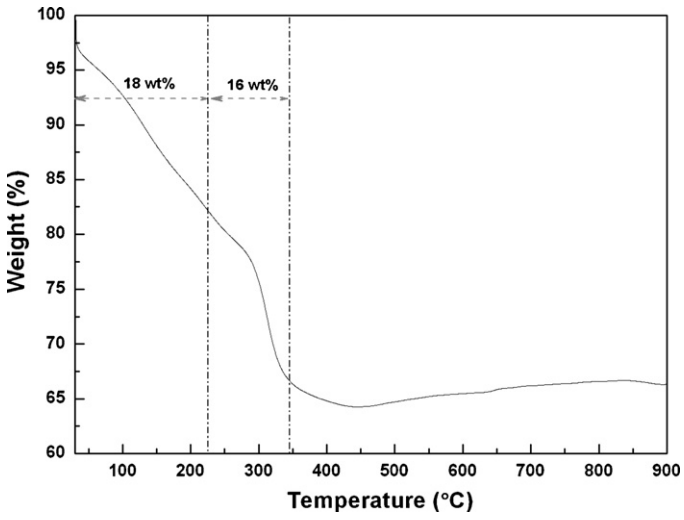

Fig. 1. TG curve of Ag/Co granular alloy. The vertical lines demarcate the region of weight losses corresponding to solvent at ~230 °C and surfactant at ~320 °C.

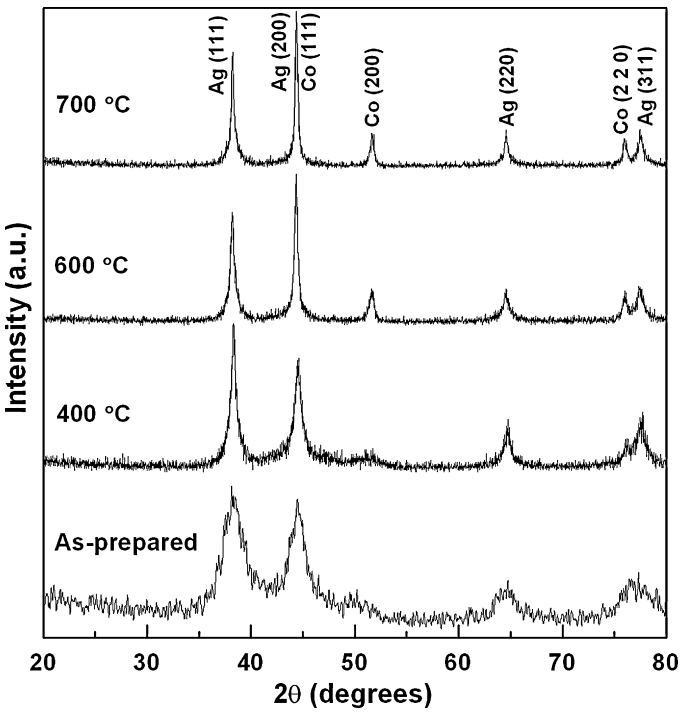

Fig. 2. Evolution of Ag/Co crystalline phases as a function of annealing temperature.

in Ar gas flow [16]. Crisan et al. [17], prepared different compositions of Ag–Co nanoparticles such as $Ag_{30}Co_{70}$ and $Ag_{55}Co_{45}$ through thermal decomposition method, in the presence of oleic acid/tri-dodecylamine as surfactants. Core–shell morphology of the Ag–Co nanoparticles having mean size of 15.2 nm with coercivity value of 150 Oe was achieved at room temperature. Similarly, Sobal et al. [18], synthesized monodisperse bimetallic Ag/Co composite nanocrystals by colloidal chemistry using tridodecylamine as a surfactant. The measured particle size for the Ag/Co particles was around 12 nm. Despite of these progresses in the synthesis of granular Ag/Co solids, a suitable method for producing single-nanometer size particles of AgCo (i.e. size of range < 10 nm) is still lacking. In this context, herein we report such an effort to yield very fine particles of Ag/Co adopting the polyol process. During our attempts to

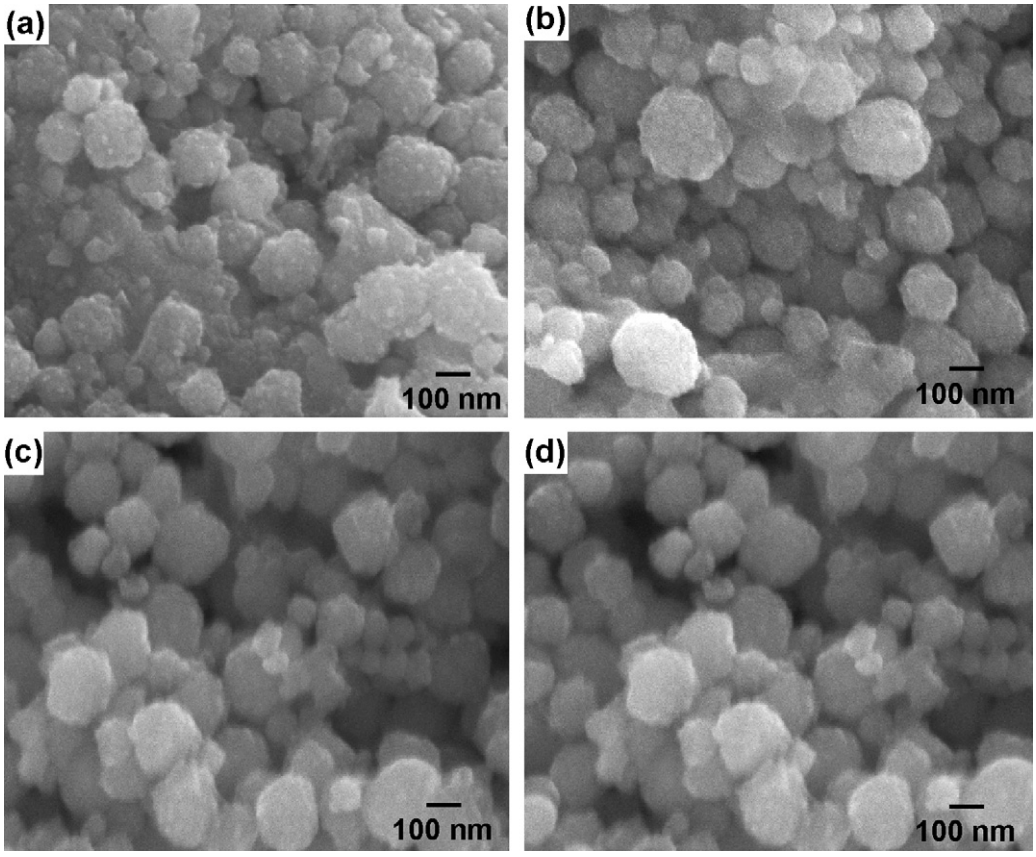

Fig. 3. FESEM micrographs of Ag/Co spherical aggregates. (a) As-prepared and (b), (c) and (d) annealed at 400, 600 and 700 °C for 1 h, respectively.

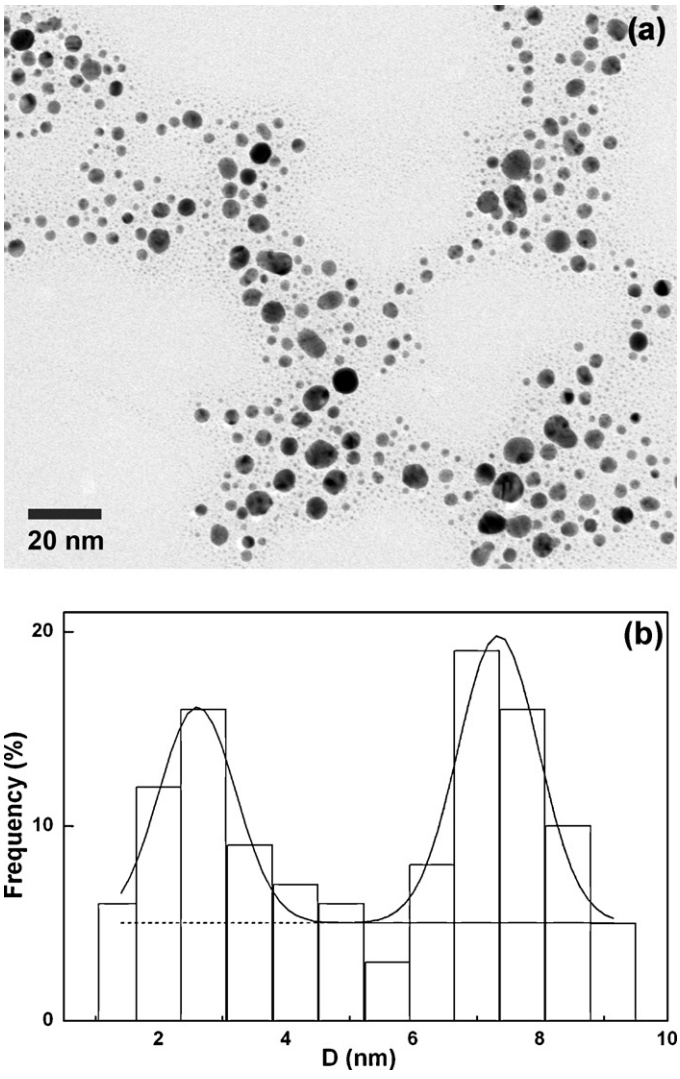

Fig. 4. (a) TEM micrograph Ag/Co bimetallic nanoparticles and (b) their corresponding histogram showing bimodal distribution of particles.

synthesize Ag/Co nanoparticles stabilized by oleic acid and oleylamine, we observed a formation of spherical granular composite structures from very fine primary Ag/Co nanoparticles. The spherical aggregates so obtained are surprisingly dense and uniform on a large-scale and could be easily dispersible in toluene and hexane. Such materials would be interesting for studying the effect of assembly and mesostructure on cooperative magnetic phenomena.

2. Experimental

Oleic acid (90%, technical grade), oleylamine (90%, technical grade), silver nitrate ($AgNO_3$, >99%) and cobalt acetate ($Co(CH_2COO)_2$; 98%) were purchased from Aldrich. Organic solvents such as ethylene glycol, ethanol and toluene used were analytical grade and obtained from various sources. All the chemicals were used as-received without any further purification.

The Ag/Co bimetallic nanoparticles were synthesized by the polyol process, i.e. simultaneous reduction of cobalt acetate and silver nitrate in a coordinating solvent containing oleic acid and oleylamine under Ar atmosphere. In a typical synthesis, a mixture of cobalt acetate (0.4 M), $AgNO_3$ (0.6 M), oleic acid/oleylamine (1:1) in 100 mL of deoxygenated ethylene glycol was heated to 200 °C under N_2 atmosphere with vigorous stirring. After 60 min of refluxing, the mixture was cooled down to room temperature and then the particles were precipitated by washing several times with ethanol and centrifuging. The supernatant was discarded by decanting. The extracted Ag/Co nanopowders can be redispersed in toluene or hexane, reversibly.

The crystal structure of the as-synthesized Ag/Co nanoparticles was characterized by X-ray powder diffractometry (XRD) (Philips, Cu-Kα radiation). Both elemental analysis and morphology of the Ag/Co nanoparticles were performed using energy dispersive X-ray (EDX) analysis attached with a field emission scanning electron microscope (FESEM/EDAX-S4300 SE/N). The actual composition of the Ag/Co nanoparticles was quantitatively determined by an inductively coupled plasma atomic emission spectrometer (ICP-AES). Transmission electron microscopy (TEM) and selected area electron diffraction (SAED) measurements were performed with a 300 kV JEOL 3010 transmission electron microscope. For UV–vis spectroscopy (UV–vis) studies, samples were dispersed in toluene and filled in 10 mm pathlength quartz cuvette and the spectra were recorded on a Perkin-Elmer Lambda 900 spectrometer using toluene, for background correction. Thermogravimetric (TG) measurements were carried out with a Mettler-Toledo instrument in the temperature range of 100–800 °C under N_2 atmosphere at a heating rate of 5 °C/min. Small angle X-ray scattering (SAXS) measurements for the Ag/Co colloidal samples were performed with the help of PW3830 X-ray generator (Anton-Paar, Austria) operated at 40 kV and 50 mA with Cu target. The scattering data collected were used to calculate size, shape and distribution of the Ag/Co nanoparticles. Data were obtained in the form of scattered X-ray intensity '*I*' as a function of the scattering vector, $q = (4\pi \sin(\theta)/\lambda)$, where θ is the scattering angle and λ is the wavelength of the incident beam [19]. The data analysis was performed using GIFT computer program. Magnetic measurements were performed with a vibrating sample magnetometer (VSM) (ADE make, model EV9) up to a maximum field of 2 T. Field cooled (FC) and zero field cooled (ZFC) thermomagnetic curves were measured from 10 to 350 K in an applied field of 100 Oe using a superconducting quantum interference device (SQUID) magnetometer.

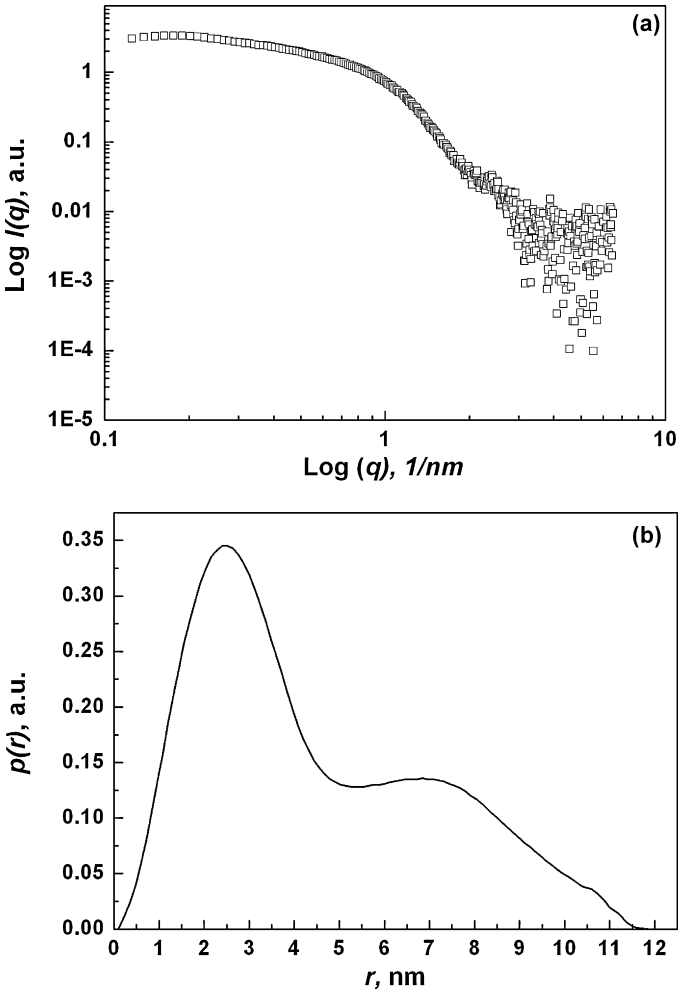

Fig. 5. Small angle X-ray scattering results for Ag/Co granular alloy. (a) Experimental scattering intensity plot: log $I(q)$ vs. scattering vector log q and (b) experimental pair distance distribution function $p(r)$ vs. radial distance r.

3. Results and discussion

The thermal stability and the weight loss occur during the heat treatment of granular Ag/Co solids were studied using thermogravimetric analysis. The TG curve for granular Ag/Co solids showed a two-step weight-decline pattern with the inflexion points at

Table 1
Crystallite size, lattice parameter, coercivity and magnetization values of Ag/Co nanoparticles processed at various annealing temperatures.

Samples of Ag/Co nanoparticles	Crystallite size, d_{xrd} (nm)		Lattice parameter (Å)		Coercivity, H_c (Oe)	Magnetization, M_s (emu/g)
	Ag	Co	Ag[a]	Co[a]		
As-prepared	4.9	8.7	4.0892	–	123	63.9
400 °C	27.7	42.3	4.0778	3.5390	151	91.9
600 °C	48.8	88.3	4.0849	3.5379	172	95.7
700 °C	–	–	4.0778	3.5395	174	100.2

[a]Lattice parameter of pure Ag: 4.0855 (JCPDS#89-3722) and pure Co: 3.5442 (JCPDS # 89-7093).

around ~230 °C and ~320 °C (Fig. 1); the former corresponding to the desorption of solvent molecules (ethylene glycol) and the latter due to the degradation of surfactant (oleic acid/oleylamine). The observed weight losses for the solvent and surfactant coating are ~18% and ~16%, respectively. The chemical composition of the Ag/Co granular solids was evaluated by both EDX and ICP-AES and the composition values are in close agreement with the expected composition (Ag: 0.6; Co: 0.4) within 1–4% error. With the ICP-AES measurements, elemental composition of 58.56 wt% (Ag) and 41.44 wt% (Co) was determined; whereas with the EDX analysis, composition of 59.21 wt% (Ag) and 40.79 wt% (Co) was estimated. Though the ICP-AES composition values are slightly lesser than that of the EDX values, the former can be considered as more quantitative in view of its sensitivity. Fig. 2 shows the XRD patterns for the granular Ag/Co solids as a function of annealing temperature. The XRD patterns of both as-prepared and annealed samples display peaks of the pure bulk-like FCC-Ag and FCC-Co phases. That is understandable since Ag and Co are immiscible. The calculated lattice parameters for the Ag and Co phases are quite comparable with of the pure Ag and Co (Table 1)—indicating that no alloy formation occurred during the synthesis. Using Scherer's equation, the average crystallite size of the as-synthesized and annealed Ag/Co samples was calculated for the Ag and Co phases and the results are listed in Table 1. The average crystallite size values obtained for the Ag and Co phases are quite different and the values which were calculated for the Co phases are significantly higher than that of the Ag phase. These observations can be substantiated with the TEM and SAXS analysis.

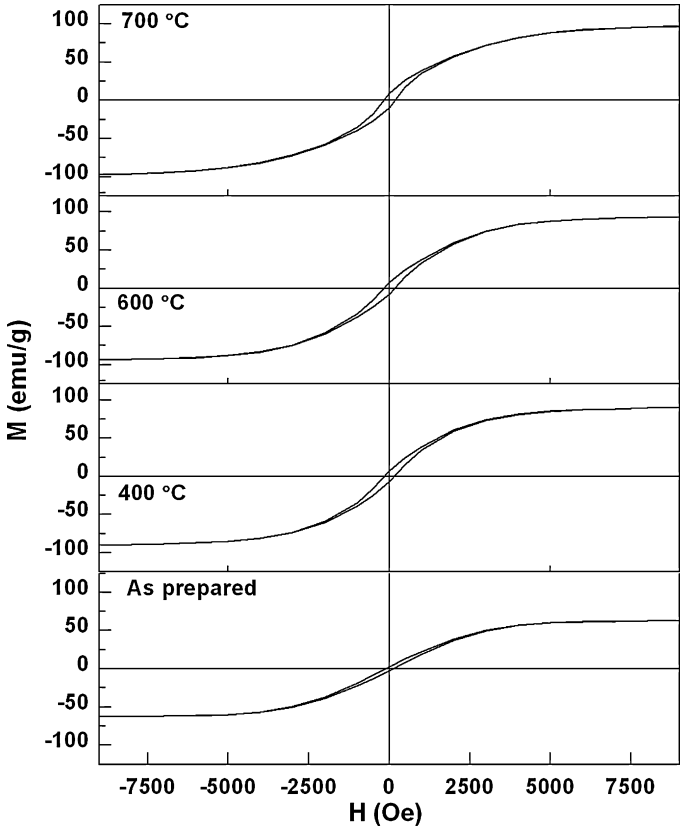

Fig. 6. Room temperature hysteresis curves of Ag/Co granular alloy samples obtained at different annealing temperatures.

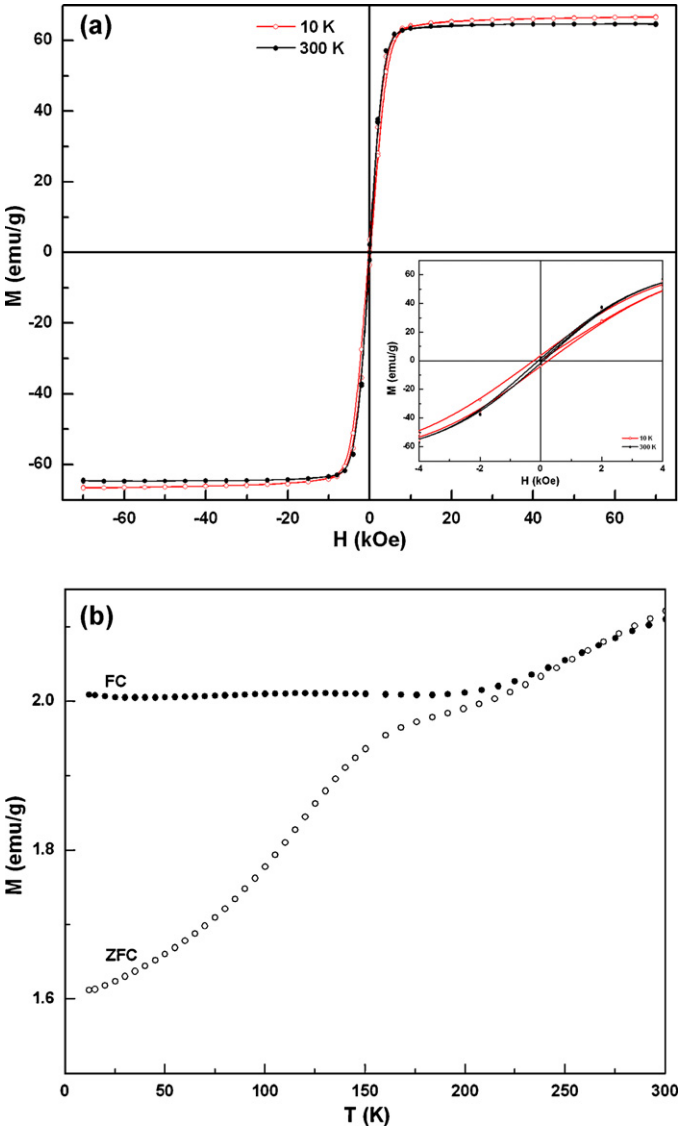

Fig. 7. (a) Magnetic field dependence of magnetization of Ag/Co nanoparticles at 5 K and 300 K. Inset shows, close view of coercivity build up at 5 K. (b) Temperature dependence of FC and ZFC dc magnetization measured under an applied magnetic field of 100 Oe.

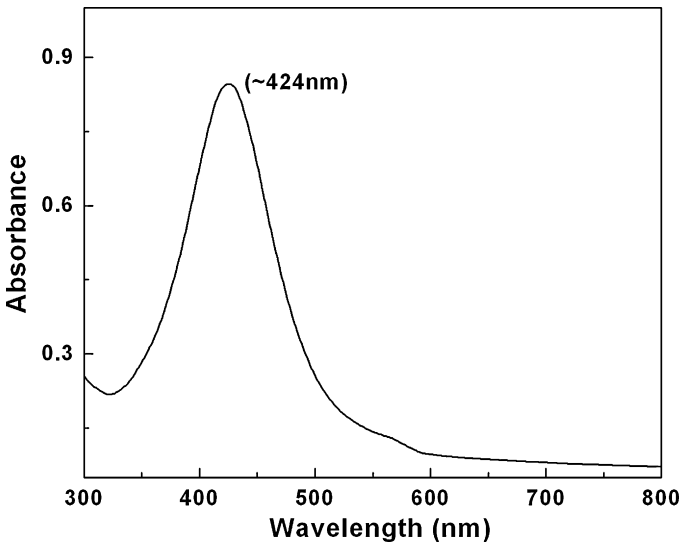

Fig. 8. UV–vis spectrum of Ag/Co bimetallic nanoparticles.

The morphology of both as-prepared and annealed Ag/Co nanopowders was studied using FESEM and the representative micrographs are shown in Fig. 3. It can be seen that a very fine agglomerated nanoparticles appear in the form of spherical granules in the size range of 50–200 nm; with each spherical granule consisting of several individual nanoparticles. The granular morphology of the Ag/Co nanoparticles did not affect with the annealing, i.e. in terms of structure and size (Fig. 3b–d). We presume that the spherical granular nature of the Ag/Co nanoparticles may be due to the strong magnetic dipolar interaction between the individual Ag and Co nanoparticles during the solvent evaporation stage and the fact can be validated with the following TEM and SAXS results. In order to observe the morphology of individual nanoparticles by TEM, a low concentrated solution of nanoparticles (1/3000) was deposited on a carbon-coated TEM grid and a typical micrograph is shown in Fig. 4a. It can be seen that the nanoparticles are non-agglomerated and spherical with diameter in the range of 2.3–8.2 nm. Besides, one can notice that there are two distinct peaks in the histogram (Fig. 4b); one is at 2.5 nm and another is at 7.4 nm—indicating the presence of bimodal distribution of nanoparticles in the as-prepared Ag/Co samples.

The existence of bimodal distribution of nanoparticles in the Ag/Co samples can be further confirmed with the SAXS analysis. The experimental scattering function $I(q)$ obtained for the as-prepared granular Ag/Co nanoparticles is shown in Fig. 5a—indicates that the shape of the particles are spherical, based on the power law [20]. The particle size calculated from the pair distance distribution function, $p(r)$, which is given by the equation [21]:

$$p(r) = \frac{1}{2\pi^2} \int I(q) \cdot qr \cdot \sin(qr) \cdot dq$$

where $p(r)$, is the pair distance distribution function, $I(q)$, is the intensity as a function of scattering vector (q); q, is the length of the scattering vector; r, is the size of particle. Fig. 5b shows the plot of $p(r)$ vs. radial distance r for the Ag/Co colloidal dispersion and it can be seen that the curves exhibit distinct peaks for the bimodal distribution of Ag/Co nanoparticles with mean particle size values of 2.4 and 7.0 nm. Since the SAXS results are considered to be much better statistical average in comparison to that of TEM results, the former exhibit the real size of the particles. Further, with the appearance of $p(r)$ vs. r curve, one can easily recognize nature of colloidal dispersion, i.e. core–shell and single metallic nanoparticles. In the case of core–shell structures, a dip in $p(r)$ vs. r curve is usually obtained—due to the change in electron density profiles of dissimilar metal systems. In the present case, two continuous peaks are seen without any dip in the curve—indicating the absence of core–shell formation in the Ag/Co colloidal dispersion [19,22].

The room temperature hysteresis curves obtained for Ag/Co granular alloy samples annealed at different temperatures are shown in Fig. 6. The hysteresis curve displays a typical ferromagnetic characteristics with saturation magnetization (M_s), remanent magnetization (M_r), and coercivity (H_c) values of 64 emu/g, ~2 emu/g and 123 Oe, respectively. Considering that there is 0.40 g Co in 1 g Ag/Co granular alloy; if it has 60% Ag atoms and 40% Co atoms, and that 1 g crystalline Co has a 161 emu saturation magnetization moment at room temperature, 0.40 g crystalline Co should have 64.4 emu magnetic moment under the intense applied field. Thus, the M_s value of 64 emu/g obtained for the as-synthesized Ag/Co nanoparticles is in quantitative agreement with the saturation magnetization deduced from the atomic ratio of sample. Further, the M_s value tends to increase with the annealing temperature; a maximum value of 100 emu/g was obtained at 700 °C. Fig. 7a shows the applied magnetic-field dependence of magnetization measured at 300 and 10 K. At temperatures of 300 K, it appears that the magnetization saturates like any ordinary ferromagnet for fields in excess of 10 kOe. However, at 10 K, the magnetization does not saturate, even at 70 kOe. This unusual behavior is due to the two component systems present in the Ag/Co granules: (i) a ferromagnetic component consisting of all the magnetic particles that exceed the critical size for ferromagnetic behavior and (ii) a paramagnetic component consisting of all magnetic particles small enough to be considered superparamagnetic or paramagnetic. At 10 K the paramagnetic component may be discerned at large magnetic fields as a non-saturating component, since its amplitude grows inversely with temperature. Fig. 7b shows the temperature dependence of FC and ZFC magnetization curves acquired for the as-synthesized Ag/Co granules with an applied magnetic field of 100 Oe. These data indicate a blocking temperature (T_B) close to 250 K. As expected for uniaxial, single-domain nanoparticles ZFC and FC curves diverge when the temperature decreases below T_B with FC that decreases smoothly towards zero values with the temperature.

At this juncture, it is very much essential to probe the nature of alloying action of Ag–Co nanoparticles, as well as their bimodal mixture. As previously mentioned in Section 1, during chemical synthesis, the formation of Ag–Co granular alloys can have three possibilities [13]: (i) core–shell type particles, Ag-core with Co-shell or vice versa [14]; (ii) phase-separated composites, which are made of partly Ag and partly of Co; and (iii) physical mixture of mono-metal particles [15]. The formation of either core–shell type of nanoparticles or the phase-separated composite cannot be assigned to the Ag/Co nanoparticles obtained with the present approach. This presumption can be probably drawn based on the UV–vis spectra obtained with the Ag/Co nanoparticles dispersion and a representative UV–Vis spectrum is shown in Fig. 8. In Fig. 8, appearance of sharp absorption peak band at ~424 can be noticed for the characteristic surface plasmon resonance of Ag nanoparticles. The occurrence of both the alloy and the core–shell structures of Ag/Co nanoparticles is usually reflected in the UV–vis spectra. In the case of core–shell type Ag/Co or phase-separated Ag/Co colloidal particles, one can expect peak broadening associated with blue shift of Ag plasmon band [18]. In the present study, neither a blue shift nor a broadening of the Ag plasmon wavelength is seen in Fig. 8; this suggests that that the Ag/Co nanoparticles prepared by the present approach are probably a physical mixture of mono-metal nanoparticles. Among the bimodal mixture of Ag and Co nanoparticles, we ascribe smaller size distribution for the Ag particles; while slightly larger size distribution for the Co particles. As the standard reduction potential (E^0) of Ag (0.80 V) is more positive than that of Co (−0.297 V), the velocity of reduction of Ag^+

ions is faster than the velocity of reduction of Co^{2+} ions. Therefore, the tendency for reduction of more number of fine particles during the polyol process is highly favorable in the case of Ag. The above fact can be apparently corroborated with the crystallite size values estimated with the XRD analysis.

The bimodal mixture of Ag/Co nanoparticles obtained in this study is in high yield and it is useful to comment on the formation of spherical aggregate structures. The driving force for stabilizing the spherical aggregates is the solvent (ethanol), which is used in the present study. This conclusion is drawn based on the following fact. Our attempts to form spherical aggregates in other solvents such as ethylene glycol failed; only discrete nanocrystals were formed. Apparently, the solvent is important for stabilizing the spherical aggregates and the aggregate structures take place only at the time of solvent evaporation stage. This may be due to the solvent–surfactant interactions that change its conformation and mobility in solution in a way that modifies its ability to induce nanoparticle aggregation [23]. Similar observations on the spherical aggregates have been earlier made in the case of Pd [24], Pt [25] and Au–Pt [26] nanoparticles.

At this stage, it is also necessary to discuss about the nature of bimodal mixture of Ag/Co nanoparticles. The agglomerates can be either mixture of Ag/Co or individual Co and Ag nanoparticles. However, we suppose that the aggregates could be probably a mixture of Ag/Co nanoparticles and not individual Ag and Co; as the recent studies on the synthesis of Ag [27] and Co [28] nanoparticles showed that there is no such evidence of obtaining spherical aggregates of individual Co or Ag nanoparticles. Further, the present synthetic approach is co-synthesis yielding both Ag and Co nanoparticles simultaneously, the dipolar interaction exists between the Ag and Co nanoparticles could be another possible reason for stabilizing the aggregates, in addition to the surfactant–solvent interactions.

4. Conclusions

Ag/Co bimetallic nanoparticles in the form of spherical aggregates were synthesized through adopting a modified polyol process, using oleic acid/oleylamine as stabilizers. Both XRD and UV–vis studies demonstrated the occurrence of individual particles of Ag and Co in the Ag/Co colloids. Formation of dense and uniform spherical aggregates was evident in the FESEM micrographs and these superstructures also appear to be thermally stable. These spherical aggregates, which generally have diameters between 50 and 200 nm, are built from primary Ag and Co particles of size 2–8 nm. Accordingly, a bimodal distribution of nanoparticles in the Ag/Co colloids was revealed by the TEM studies and these results were substantiated with the SAXS analysis, in terms of both particle size and distribution. Magnetic measurements showed typical ferromagnetic characteristics for the as-prepared Ag/Co nanoparticles with blocking temperature close to 250 K. The nanoparticle aggregates, such as those obtained in the present study could be important systems for studying the influence of catalytic activity and cooperative magnetic properties on interparticle separation and nanostructure.

Acknowledgments

The financial support for the present study was extended by Defence Research and Development Organization (DRDO), Government of India. The keen interest shown by the Director, DMRL in this work is gratefully acknowledged.

References

[1] S. Kenane, J. Voiron, N. Benbrahim, E. Chainet, F. Robaut, J. Magn. Magn. Mater. 297 (2006) 99–106.
[2] Y. Kong, H.B. Guo, H.F. Yan, B.X. Liu, J. Phys. Chem. B 109 (2005) 9362–9367.
[3] L. Piraux, M. Cassart, J.S. Jiang, J.Q. Xiao, C.L. Chien, Phys. Rev. B 48 (1993) 638–641.
[4] W. Zhang, I.W. Boyd, M. Elliott, W. H-Harkerand, J. Magn. Magn. Mater. 165 (1997) 330–333.
[5] S.H. Liou, S. Malhotra, Z.S. Shan, D.J. Sellmyer, S. Nafis, J.A. Woollarn, C.P. Reed, G.M. Chow, R.J. Deangelis, J. Appl. Phys. 70 (1991) 5882–5884.
[6] M. Kitada, J. Mater. Sci. Lett. 13 (1994) 500–502.
[7] M.P. Andrews, S.C. O'Brien, J. Phys. Chem. 96 (1992) 8233–8241.
[8] H. Zaman, A. Yamada, H. Fukuda, Y. Ueda, J. Electrochem. Soc. 145 (1998) 565–568.
[9] T.J. Jackson, S.B. Palmer, H.J. Blythe, A.S. Halim, J. Magn. Magn. Mater. 159 (1996) 269–281.
[10] D. Jingfa, Z. Xiping, M. Enze, Appl. Catal. 37 (1988) 339–343.
[11] L.Z. Mezey, J. Giber, Jpn. J. Appl. Phys. 21 (1982) 1569–1571.
[12] L.J. Huang, E. Ma, B.X. Liu, Phys. Status Solidi A 110 (2006) 443–448.
[13] T. Van Hoof, A. Dzhurakhalov, M. Hou, Eur. Phys. J. D 43 (2007) 159–163.
[14] M. Chen, L. Gao, Inorg. Chem. 45 (2006) 5145–5149.
[15] L. Dimesso, G. Miehe, H. Fuess, H. Hahn, J. Magn. Magn. Mater. 191 (1999) 162–168.
[16] V. Chandra, R. Srivastava, S.S. Manoharan, J. Magn. Magn. Mater. 320 (2008) 2397–2401.
[17] O. Crisan, M. Angelakeris, K. Simeonidis, Th. Kehagias, Ph. Komninou, M. Giersig, N.K. Flevaris, Acta Mater. 54 (2006) 5251–5260.
[18] N.S. Sobal, M. Hilgendorff, H. Mohwald, M. Giersig, Nano Lett. 2 (2002) 621–624.
[19] O. Glatter, O. Kratky, Small Angle X-ray Scattering, Academic Press Inc., London, 1982.
[20] O. Glatter, J. Appl. Crystallogr. 10 (1977) 415–421.
[21] A. Bergmann, G. Fritz, O. Glattter, J. Appl. Crystallogr. 33 (2000) 1212–1216.
[22] C. Revenant-Brizard, J.P. Simon, J.R. Regnard, I. Manzini, B. Rodmacq, J. Appl. Crystallogr. 31 (1998) 783–788.
[23] T.D. Ewers, A.K. Sra, B.C. Norris, R.E. Cable, C.-H. Cheng, D.F. Shantz, R.E. Schaak, Chem. Mater. 17 (2005) 514–520.
[24] K. Naka, H. Itoh, Y. Chujo, Nano Lett. 2 (2002) 1183–1186.
[25] H.-P. Liang, H.-M. Zhang, J.-S. Hu, Y.-G. Guo, L.-J. Wan, C.-L. Bai, Angew. Chem. Int. Ed. 43 (2004) 1540–2153.
[26] G. Schmid, A. Lehnert, J.-O. Malm, J.-O. Bovin, Angew. Chem. Int. Ed. 30 (1991) 874–876.
[27] D.D. Evanoff Jr., G. Chumanov, ChemPhysChem 6 (2005) 1221–1231.
[28] C.W. Kim, H.G. Cha, Y.H. Kim, A.P. Jadhav, E.S. Ji, D.I. Kang, Y.S. Kang, J. Phys. Chem. C 113 (2009) 5081–5086.